Geoscience Frontiers 12 (2021) 405–414

Contents lists available at ScienceDirect

Geoscience Frontiers

journal homepage: www.elsevier.com/locate/gsf

Research Paper

Stochastic seismic slope stability assessment using polynomial chaos expansions combined with relevance vector machine

Qiu-Jing Pan [a,b], Yat-Fai Leung [b,*], Shu-Chien Hsu [b]

[a] School of Civil Engineering, Central South University, No.22, Shaoshan South Road, Changsha, 410075, China
[b] Department of Civil and Environmental Engineering, The Hong Kong Polytechnic University, Hung Hom, Hong Kong, China

ARTICLE INFO

Keywords:
Earthquake
3D slope stability
Failure probability
Seismic displacements
Seismic hazard analysis

ABSTRACT

This paper presents probabilistic assessment of seismically-induced slope displacements considering uncertainties of seismic ground motions and soil properties. A stochastic ground motion model representing both the temporal and spectral non-stationarity of earthquake shakings and a three-dimensional rotational failure mechanism are integrated to assess Newmark-type slope displacements. A new probabilistic approach that incorporates machine learning in metamodeling technique is proposed, by combining relevance vector machine with polynomial chaos expansions (RVM-PCE). Compared with other PCE methods, the proposed RVM-PCE is shown to be more effective in estimating failure probabilities. The sensitivity and relative influence of each random input parameter to the slope displacements are discussed. Finally, the fragility curves for slope displacements are established for site-specific soil conditions and earthquake hazard levels. The results indicate that the slope displacement is more sensitive to the intensities and strong shaking durations of seismic ground motions than the frequency contents, and a critical Arias intensity that leads to the maximum annual failure probabilities can be identified by the proposed approach.

1. Introduction

Assessment of slope stability under earthquake excitations is a challenging problem in geotechnical engineering. Previous methods developed for such purpose can be broadly categorized into three groups (Jibson, 2011): (1) pseudostatic analysis, (2) stress-deformation analysis and (3) Newmark-type displacement analysis. The pseudostatic approach, which simplifies seismic excitations as constant inertial forces, is commonly used in the slope engineering practice. Although the approach is straightforward and easily implementable, it fails to represent the dynamic nature of earthquake motions and the results obtained are either pseudostatic safety factors or critical seismic accelerations (Qin and Chian, 2018). However, the displacements experienced by the slopes are often more important from the perspective of hazard management (Lin and Whitman, 1986). While stress-deformation analyses using finite element methods provide the most realistic representation of slope behavior subjected to seismic loadings, these often involve complex modeling techniques, such as determination of boundary conditions and selection of constitutive models, and are usually computationally demanding (Li et al., 2018).

The Newmark's sliding block analysis method (Newmark, 1965; Jibson, 2011) incorporates the dynamic nature of ground motions in a more realistic manner than pseudostatic analysis, but is not as sophisticated as finite element simulation. It captures the essence in slope deformation during earthquakes, and has been widely adopted by many researchers, such as (Hsieh and Lee, 2011; Nadukuru and Michalowski, 2013; Chousianitis et al., 2014; He et al., 2015; Tasi and Chien, 2016; Leshinsky, 2018). In these studies, recorded ground motions were used to evaluate slope displacements and empirical equations were built correspondingly by regression analysis, but they did not explicitly consider different levels of uncertainties regarding soil properties, slope geometries and earthquake ground motion features (intensity, frequency and duration).

On the contrary, probabilistic analyses allow these uncertainties to be incorporated rationally and quantitatively, and expressed as failure probabilities or hazard levels. Meanwhile, it should be noted that ground motion records from previous earthquake events are not always applicable for stochastic analysis. Although some regression formulas had been directly adopted in probabilistic analysis (Travasarou et al., 2004; Du and Wang, 2016), their validity is questionable at regions where the

* Corresponding author.
E-mail address: andy.yf.leung@polyu.edu.hk (Y.-F. Leung).
Peer-review under responsibility of China University of Geosciences (Beijing).

https://doi.org/10.1016/j.gsf.2020.03.016
Received 6 October 2019; Received in revised form 16 January 2020; Accepted 22 March 2020
Available online 18 April 2020

regression data are scarce. Besides, many of these regression formulas only adopt one or two ground motion parameters for prediction of slope displacements, which are in fact affected by multiple earthquake ground motion characteristics, including the intensity, frequency content and duration. An alternative approach is to generate synthetic ground motions. Some simplified methods, such as sinusoidal curves or Gaussian stationary process (Lin and Whitman, 1986; Kim and Sitar, 2013; Qin and Chian, 2018), had been used to simulate seismic ground motions in previous probabilistic slope stability analysis. These simplified methods either involve parameters without clear physical meaning or hardly represent realistic earthquake ground motions.

The current study adopts the stochastic ground motion model proposed by Rezaeian (2010), which is capable of simulating both the temporal and spectral non-stationary characteristics of earthquake shakings in a more realistic manner than simplified ground motion models. Besides, the metamodeling method of polynomial chaos expansion (PCE) has been widely employed to conduct probabilistic analysis in geotechnical engineering (e.g. Mollon et al., 2010; Li et al., 2011; Lo and Leung, 2017, 2018; Guo et al., 2018; Pan et al., 2020). However, PCEs suffer from a substantial computational burden, especially for high-dimensional problems. In order to enhance the computational efficiency, sparse polynomial chaos expansions (SPCEs) have recently gained popularity (e.g., Blatman and Sudret, 2010; Xu and Kong, 2018). Relevance Vector Machine (RVM) is a machine learning technique which adopts Bayesian inference method to obtain sparse solutions for regression or classification problems (Tipping, 2001). In this work, a novel method is proposed to incorporate SPCE with RVM, in an attempt to perform probabilistic analyses of slope stability considering stochastic seismic ground motions.

In the subsequent sections, the Rezaeian's stochastic ground model is introduced, followed by evaluation of the Newmark-type slope displacement with the three-dimensional rotational failure mechanism. The methods of PCE (metamodeling) and RVM (machine learning) are then introduced. The presented RVM-PCE is compared with other methods in terms of the evaluated failure probabilities. A sensitivity analysis and a parametric study are then conducted to elucidate the influences of ground motion parameters on slope displacements. Finally, the fragility curves and hazard curves of slope displacements are generated by combining various sources of uncertainty.

2. Artificial ground motion models

Real earthquake ground motions are associated with both temporal (in the time domain) and spectral nonstationary (in the frequency domain) features (Rezaeian, 2010), and a good artificial stochastic ground motion model should be able to simulate both characteristics. Temporal nonstationarity refers to the evolving intensities of ground motions in time, which increases slowly from zero to a nearly constant value ("strong shaking" phase of an earthquake) and then decreases back to zero during a total of approximately 10–60 s; spectral nonstationarity refers to time-varying frequencies of ground motions, starting with high frequencies (short wavelengths) during the initial few seconds, followed by moderate frequencies (moderate wavelengths) and ending with low frequencies (long wave lengths) (Rezaeian, 2010).

Rezaeian and Der Kiureghian (2008) proposed a synthetic ground motion model which adopts a modulated filtered white-noise process to achieve the temporal and spectral nonstationarity. In their model, time-modulating functions and linear filters are employed to shape the random process in the time and frequency domains, and a synthetic seismic acceleration time-history $a(t)$ is given by

$$a(t) = q(t,\ \boldsymbol{\alpha})\left\{\frac{1}{\sigma_h}\int_{-\infty}^{t} h[t-\tau,\boldsymbol{\lambda}(\tau)]\omega(\tau)d\tau\right\} \tag{1}$$

where $\omega(\tau)$ is a white-noise process; σ_h is a normalization term; the gamma time-modulating function $q(t,\boldsymbol{\alpha})$ is defined as

Table 1
Statistics of six ground motion parameters (Rezaeian, 2010).

Ground motion parameters	Probability Distributions	Mean (μ)	COV	Distribution Bounds
I_a (m/s)	Lognormal	0.05	3.5	[0, ∞]
$D_{5\text{-}95}$ (s)	Beta	17.25	0.5	[5, 45]
t_{mid} (s)	Beta	12.38	0.6	[0.5, 40]
$\omega_{mid}/2\pi$ (Hz)	Gamma	5.87	0.5	[0, ∞]
$\omega'/2\pi$ (Hz)	Two-sided Truncated Exponential	−0.09	2.1	[−2, 0.5]
ζ_f	Beta	0.21	0.7	[0.02, 1]

$$q(t,\boldsymbol{\alpha}) = \alpha_1 t^{\alpha_2-1}e^{-\alpha_3 t} \tag{2}$$

in which the vector $\boldsymbol{\alpha} = \{\alpha_1,\ \alpha_2,\ \alpha_3\}$ determines the intensity, shape and duration of the process; the single-degree-of-freedom linear filter $h[t-\tau,\boldsymbol{\lambda}(\tau)]$ is defined as

$$h[t-\tau,\boldsymbol{\lambda}(\tau)] = \begin{cases} \dfrac{\omega(\tau)}{\sqrt{1-\zeta^2(\tau)}}e^{-\zeta(\tau)\omega(\tau)(t-\tau)}\sin\left[\omega(\tau)(t-\tau)\sqrt{1-\zeta^2(\tau)}\right], \tau \le t \\ 0,\ \tau > t \end{cases} \tag{3}$$

where $\boldsymbol{\lambda}(\tau) = [\omega(\tau),\ \zeta(\tau)]$, with $\omega(\tau)$ and $\zeta(\tau)$ representing the predominant frequency and the damping ratio, respectively.

Some key physical features of an earthquake ground motion that impact structure responses include the time-varying intensity, the effective duration, the evolving predominant frequency and the bandwidth of motions. Six physically based parameters (I_a, $D_{5\text{-}95}$, t_{mid}, ω_{mid}, ω', ζ_f) are employed to characterize ground motions (Rezaeian, 2010). In the modulated filtered white-noise process model, the intensity-related parameters $\boldsymbol{\alpha}$ and frequency-related parameters $\boldsymbol{\lambda}(\tau)$ can be calibrated by these six ground motion physical parameters.

The intensity-related parameter vector $\boldsymbol{\alpha} = \{\alpha_1,\ \alpha_2,\ \alpha_3\}$ can be determined by three physical parameters (I_a, $D_{5\text{-}95}$, t_{mid}). The first physical parameter I_a is the Arias intensity, which is defined as the time-integral of the square of the ground acceleration time-histories:

$$I_a = \frac{\pi}{2g}\int_0^{T_d} a(t)^2 dt \tag{4}$$

where g is the gravitational acceleration and T_d the total motion duration. The Arias intensity is often deemed as the most suitable and reliable indicator to represent the damaging effects of earthquake shakings, since it incorporates the features of shaking amplitude and duration of ground motions, and provides the complete energy content of seismic waves propagating inside soil masses (Chousianitis et al., 2014). Therefore, it carries more information than a single peak value, such as peak ground accelerations or peak ground velocity.

The second physical parameter $D_{5\text{-}95}$ was defined by Rezaeian (2010) as the time interval between the instants at which 5% and 95% of the expected Arias Intensity are reached, representing the strong shaking phase. The third parameter t_{mid} is the time at which 45% of the expected Arias Intensity is reached during the strong shaking phase. The evolving predominant frequency $\omega(\tau)$ is assumed to be linearly varying, which can be determined by two physical parameters ω_{mid} and ω', which respectively defines the filter frequency at t_{mid} and its changing rate. The filter damping ratio $\zeta(\tau)$ is taken as a constant ζ_f. The details on the determination of parameters $\boldsymbol{\alpha}$ and $\boldsymbol{\lambda}(\tau)$ using (I_a, $D_{5\text{-}95}$, t_{mid}, ω_{mid}, ω', ζ_f) can be found in Rezaeian (2010). Thus an artificial ground motion can be simulated with the modulated filtered white-noise process model for a specified set of ground motion parameters.

Rezaeian (2010) estimated the statistical properties of the six physical parameters of seismic ground motions, based on 206 data points from the Campbell-Bozorgnia NGA database (Campbell and Bozorgnia, 2007, 2008), which contain 31 pairs of horizontal recordings from 12 earthquakes for

Table 2
Correlation coefficients between six ground motion parameters (after Rezaeian, 2010).

	I_a	$D_{5\text{-}95}$	t_{mid}	ω_{mid}	ω'	ζ_f
I_a	1	−0.36	0.01	−0.15	0.13	−0.01
$D_{5\text{-}95}$	−0.36	1	0.67	−0.13	−0.16	−0.2
t_{mid}	0.01	0.67	1	−0.28	−0.2	−0.22
ω_{mid}	−0.15	−0.13	−0.28	1	−0.2	0.28
ω'	0.13	−0.16	−0.2	−0.2	1	−0.01
ζ_f	−0.01	−0.2	−0.22	0.28	−0.01	1

strike-slip type of faulting, and 72 pairs of horizontal recordings from 7 earthquakes for reverse type of faulting. These statistical properties, including mean values, coefficients of variation (COVs), probability distributions, are listed in Table 1, and their correlation coefficients are given in Table 2. These values are adopted in this paper. Fig. 1 shows two artificial ground motion records for two cases of Arias intensity, with the other ground motion parameters corresponding to the means values given in Table 1. The two acceleration time histories involve similar durations, predominant frequencies and bandwidths at the strong shaking phase, but very different peak ground accelerations due to different Arias intensities.

3. Newmark displacements for 3D slope failure mechanisms

Newmark-type displacement approach presumes that permanent displacements of slopes occur when the earthquake ground acceleration exceeds a critical value, which may be obtained by the pseudostatic analysis, and the failing mass is treated as a sliding block moving on a given failure surface. The magnitude of total displacements is obtained by double integration of the difference between the ground motion and the critical accelerations with respect to time. This paper estimates seismic slope displacements by combining the Newmark-type method with the kinematical approach of limit analysis.

Slope analysis based on the kinematical approach of limit analysis has attracted considerable attention over the years, and the three-dimensional rotational failure mechanism is a classical model for slope stability analysis, which inspired many subsequent works (Michalowski and Drescher, 2009; Zhao et al., 2016; Huang et al., 2018). It can be easily incorporated into the pseudostatic analysis to estimate safety factors of slopes (Michalowski and Martel, 2011; Yang and Pan, 2015), and into the Newmark-type displacement analysis of slopes (Nadukuru and Michalowski, 2013; He et al., 2015). The rotational failure mechanism of a 3D slope model, with a height H, a width B and an inclination angle β, subjected to earthquake ground motions, is shown in Fig. 2. More details on the rotational mechanism are available in Michalowski and Drescher (2009). Pan et al. (2017) presented a discretization scheme for the failure mass under this mechanism, which is employed herein to evaluate the Newmark-type displacements, following the similar procedure as Nadukuru and Michalowski (2013). The current work extends the study of Nadukuru and Michalowski (2013) by incorporating stochastic seismic ground motions to slope displacement estimates in the probabilistic framework.

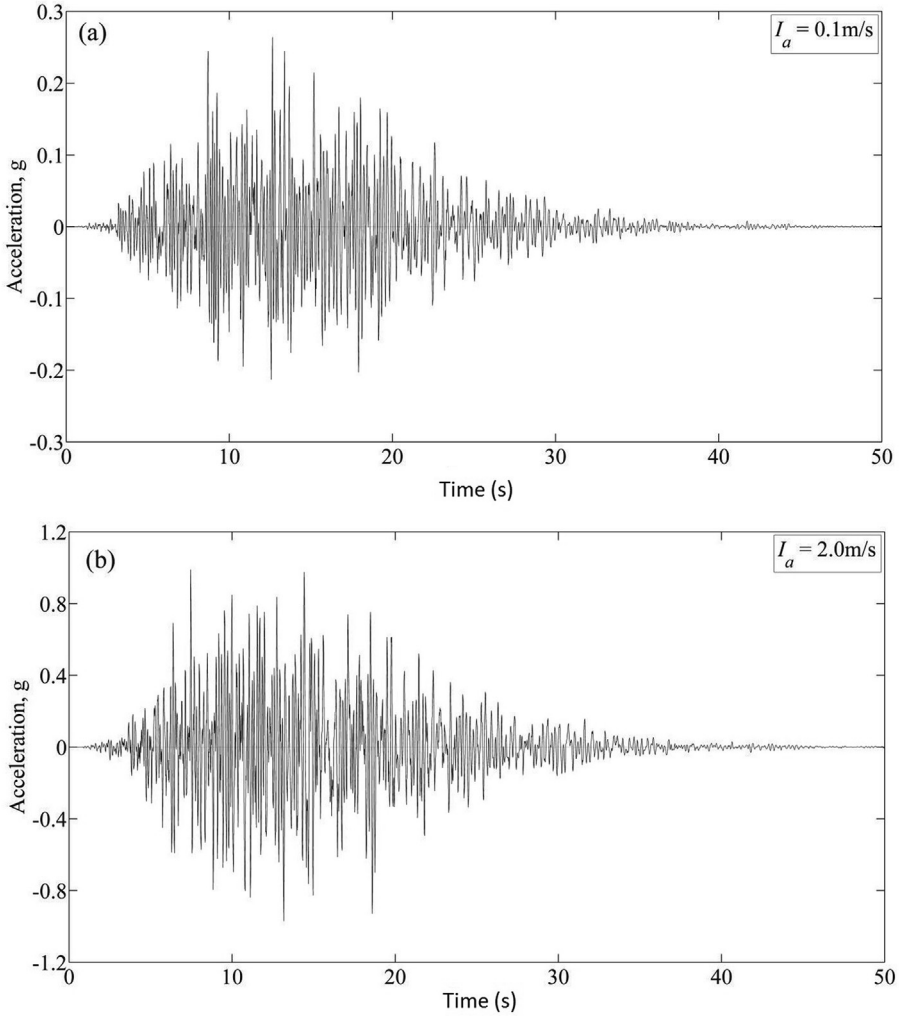

Fig. 1. Simulated ground motion records by Rezaeian's stochastic model for (a) I_a = 0.1 m/s and (b) I_a = 2.0 m/s.

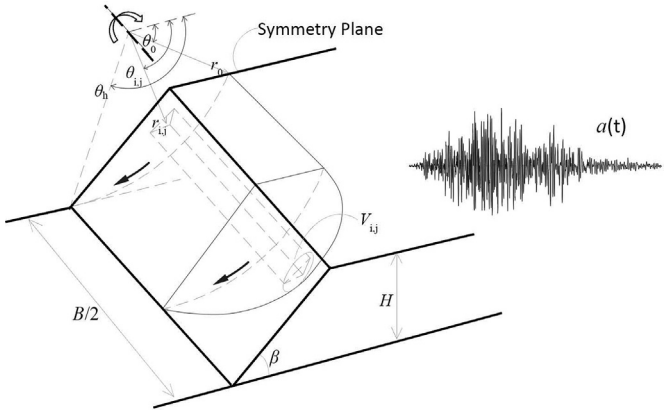

Fig. 2. Rotational failure mechanism of a 3D slope.

Table 3
Geometry and shear strength parameters of two example slopes.

Parameters	Slope A			Slope B		
	Mean (μ)	COV	Correlation coefficient	Mean (μ)	COV	Correlation coefficient
β (°)	60	0	–	48	0	–
H (m)	12	0	–	12	0	–
B/H	3	0	–	5	0	–
γ	20	0	–	20	0	–
c (kPa)	30	0.2	$\rho_{c,\varphi} = -0.5$	10	0.2	$\rho_{c,\varphi} = -0.5$
φ (°)	20	0.1		27	0.1	

The Newmark-type displacement at the slope toe is obtained by

$$S = r_0 e^{(\theta_h-\theta_0)\tan\varphi} \cdot \iint \ddot{\theta}\, dtdt, \quad \dot{\theta} > 0 \tag{5}$$

where $\ddot{\theta}$ is the block rotational acceleration,

$$\ddot{\theta} = \frac{a(t)-a_c}{I_O}\gamma\sum_i\sum_j\left(V_{i,j}r_{i,j}\sin\theta_{i,j}\right) \tag{6}$$

and a_c is the pseudostatic critical seismic acceleration:

$$a_c = \frac{-c\cot\varphi\left[\sum_{i,j}r_{i,j}s_{i,j}\cos\theta_{i,j}+\sum_{i,j}r_{i,j}s_{i,j}\cos\left(\theta_{i,j}+\beta\right)\right]-\gamma\sum_i\sum_j\left(r_{i,j}V_{i,j}\cos\theta_{i,j}\right)}{\gamma\sum_i\sum_j\left(V_{i,j}r_{i,j}\sin\theta_{i,j}\right)}g \tag{7}$$

where $(\theta_{i,j}, r_{i,j})$ are the polar coordinates of the barycenter of a discretized element, and $(V_{i,j}, s_{i,j})$ are the corresponding volume and lateral area; $I_O = \gamma\sum_i\sum_j(V_{i,j}r_{i,j}^2)/g$ is the mass moment of inertia around the rotating axis, which is treated approximately in Nadukuru and Michalowski (2013), neglecting the moment of inertia term about the mass center; g is the gravitational acceleration; γ is the soil unit weight; c and φ are the cohesion and friction angle; the geometrical parameters r_0, θ_0, θ_h, as illustrated in Fig. 2, are determined by optimizing the upper-bound solution of a_c through equating the external work rates to the internal energy dissipations.

Two example slopes with configurations listed in Table 3 are considered in this paper. The soil cohesion and friction angle are assumed to follow lognormal distributions with a correlation coefficient of −0.5, while the slope geometry (β, H, B/H) and the soil unit weight γ are taken to be deterministic because they can be easily and reliably measured. In total, there are eight input random variables, including six ground motion parameters (I_a, $D_{5\text{-}95}$, t_{mid}, ω_{mid}, ω', ζ_f) and two soil shear strength parameters (c, φ). Probabilistic analyses are then performed to study the influences of their variations on seismic slope stability.

4. Metamodel-based Monte Carlo Simulations

Probabilistic analysis is commonly adopted to quantify the effects of uncertainties associated with input parameters, by evaluating the corresponding failure probabilities of the system responses. Specifically, input parameters are often treated as random variables following prescribed probability distributions. The failure probability of model responses can be expressed by

$$P_f = \int_{G(\boldsymbol{x})\le 0} f(\boldsymbol{x})d\boldsymbol{x} \tag{8}$$

in which $\boldsymbol{x}$ is a random vector representing input parameters; $f(\boldsymbol{x})$ is the joint probability density function (PDF) of $\boldsymbol{x}$; $G(\boldsymbol{x})$ is the limit state function, with $G(\boldsymbol{x})<0$ defining failure domains. The limit state function in terms of permanent displacements of a slope is defined by

$$G(\boldsymbol{x}) = S^{max} - S(\boldsymbol{x}) \tag{9}$$

where S is the permanent displacement computed by Eq. (5), and S^{max} is the allowable permanent displacement of the slope. In order to correlate the seismic slope displacements to subsequent landslides, Jibson (2011) conducted a literature review on the thresholds of seismic slope displacements and their risk levels leading to a landslide, as summarized in Table 4. Based on their review, it appears that the threshold of 10 cm

Table 4
Summary of seismic slope displacement thresholds and associated risk levels.

References	Site location/conditions	Displacement thresholds causing landslides and damage
Wieczorek et al. (1985)	San Mateo County, California	5 cm
Keefer and Wilson (1989)	Southern California	10 cm
Jibson and Keefer (1993)	Mississippi Valley	5–10 cm
Blake (2002)	Southern California, slip surfaces intersecting stiff improvements (buildings, pools, etc.)	<5 cm
	Southern California, ductile (non-strain-softening) soils	<15 cm
	Southern California, significant strain softening soils	5 cm for peak shear strength 15 cm for residual strengths
California Geological Sudret (2008)	California	0–15 cm, serious landslide movement and damage 15–100 cm, strength loss and continuing failure >100 cm, damaging landslide movement
Jibson et al. (2000)		2–15 cm, smaller, shallow landslides
Jibson and Michael (2009)	Anchorage, Alaska	0–1 cm, low hazard 1–5 cm, moderate hazard 5–15 cm, high hazard >15 cm, very high hazard

corresponds to a moderate level of landslide risks. Thus, the allowable permanent displacement is taken as 10 cm in this study.

The calculation of Eq. (8) is generally computationally intractable, especially for high-dimensional problems. Some approaches are proposed to evaluate the failure probability approximately. These include the first-order and second-order reliability methods, Monte Carlo Simulations (MCS), response surface methods, etc., among which the MCS is a relatively straightforward and robust method. In MCS, an unbiased estimate of the failure probability is evaluated by

$$\widehat{P}_f = \frac{1}{N_{\mathrm{mc}}} \sum_{i=1}^{N_{\mathrm{mc}}} I(G(\boldsymbol{x})) \tag{10}$$

where N_{mc} is the number of samples in MCS; $I(G)$ is equal to 1 for $G < 0$, otherwise $I(G) = 0$. The coefficient of variation (COV) of estimated failure probability is expressed as

$$COV_{\widehat{P_f}} = \sqrt{\frac{1 - \widehat{P_f}}{N_{\mathrm{mc}} \widehat{P_f}}} \tag{11}$$

The classical Monte Carlo Simulation is often regarded as a standard reference for testing other probabilistic methods. However, it suffers from a rather low computational efficiency. For example, it requires 10^{k+2} simulations, according to Eq. (11), when the estimated failure probability is 10^{-k} for a coefficient of variation ($COV_{\widehat{P_f}}$) of 10%. Recently, a metamodel-based MCS technique has been proposed to circumvent this issue. The key idea is to replace the original deterministic model, for example the slope displacement S by Eqs. (5)–(7), with a metamodel in Monte Carlo Simulations. A metamodel should be computationally efficient and capable of capturing the behavior of model responses so that it can surrogate the original models to make predictions.

Several types of metamodels have been adopted in civil and geotechnical applications, such as PCE, Kriging and support vector machines (Zhang and Goh, 2013; Pan and Dias, 2017; Wan et al., 2017; Al-Bittar et al., 2018; Guo et al., 2018). PCE has been widely used in geotechnical reliability analysis as it can provide multiple aspects of probabilistic assessment, including failure probabilities, probability distribution, and statistical moments (mean, standard deviation, skewness and kurtosis) of system response. Also, it is possible to utilize the PCE to implement global sensitivity analysis based on the definition of Sobol' indices.

5. Polynomial chaos expansion

5.1. Polynomial chaos representation of model responses

If the input of a computational model $\mathscr{M}$, such as Eq. (5), are described by independent random variables gathered in an input vector $\boldsymbol{x} = \{x_1, x_2, \ldots, x_D\}^{\mathrm{T}} \in \mathbb{R}^D$, a polynomial chaos expansion of the associated model response y reads (Ghanem and Spanos, 2003; Sudret, 2008):

$$y = \mathscr{M}(\boldsymbol{x}) \cong \widehat{\mathscr{M}}_P = \sum_{i=0}^{P} w_i \psi_i(\boldsymbol{x}) \tag{12}$$

where D represents the problem dimension; w_is are polynomial coefficients; $\psi_i(\boldsymbol{x})$s are basis functions of multivariate polynomials which are tensor product of univariate polynomials. The expressions of univariate polynomials are related to the distributions of random variables, such as Hermite polynomials for Gaussian distributions, Laguerre polynomials for Gamma distributions. For example, the first four degrees of univariate Hermite polynomials are: $\psi_0 = 1, \psi_1(x) = x, \psi_2(x) = x^2 - 1$, $\psi_3(x) = x^3 - 3x$. When random variables follow non-normal distributions, the isoprobabilistic transformation is used to convert them into standard Gaussian variables; if random variables are correlated, the Cholesky decomposition is adopted.

For practical applications, a PCE is often truncated to retain a limited number of terms. The common truncation scheme requires that the total degree of univariate polynomials that constitutes the multivariate polynomials is not greater than a give PCE order p, and it leads to the total number of PCE terms $P+1$ being computed by

$$P + 1 = \frac{(D + p)!}{D! p!} \tag{13}$$

There are mainly three approaches to compute PCE coefficients, namely the intrusive method, the projection method and the regression method, among which the regression method is widely adopted in the geotechnical community due to its convenience. In the regression method, N realizations of the input vectors, denoted by a matrix $\mathbf{X} = \{\boldsymbol{x}^1, \boldsymbol{x}^2, \ldots, \boldsymbol{x}^N\}^{\mathrm{T}}$ and also termed as design of experiments (DoE), is considered. This leads to a system of linear equations with respect to PCE coefficients $\boldsymbol{w} = \{w_0, \ldots, w_P\}^{\mathrm{T}}$,

$$\begin{bmatrix} \psi_0(\boldsymbol{x}^1) & \cdots & \psi_P(\boldsymbol{x}^1) \\ \vdots & \ddots & \vdots \\ \psi_0(\boldsymbol{x}^N) & \cdots & \psi_P(\boldsymbol{x}^N) \end{bmatrix} \begin{bmatrix} w_0 \\ \vdots \\ w_P \end{bmatrix} = \begin{bmatrix} y_0 \\ \vdots \\ y_N \end{bmatrix} \tag{14}$$

where the vector $\boldsymbol{y} = \{y_1, y_2, \ldots, y_N\}^{\mathrm{T}}$ denotes the corresponding model responses. Thus the unknown PCE coefficients can be estimated by least-square minimization as follows,

$$\widehat{\boldsymbol{w}} = (\boldsymbol{\Psi}^T \boldsymbol{\Psi})^{-1} \boldsymbol{\Psi}^{\mathrm{T}} \boldsymbol{y} \tag{15}$$

where $\boldsymbol{\Psi}$ is the design matrix of polynomials basis,

$$\boldsymbol{\Psi} = \begin{bmatrix} \psi_1(\boldsymbol{x}^1) & \cdots & \psi_P(\boldsymbol{x}^1) \\ \vdots & \ddots & \vdots \\ \psi_1(\boldsymbol{x}^N) & \cdots & \psi_P(\boldsymbol{x}^N) \end{bmatrix} \tag{16}$$

In order to make the solution more stable and independent of DoE samples, a large number of DoE samples are required. Generally, the DoE size is set to be no less than two or three times P for a well-posed regression result (Blatman and Sudret, 2010).

5.2. Error estimates

The mean-square residual error is estimated to measure the fitting accuracy of a PCE metamodel on the DoE samples $\mathbf{X}$,

$$\varepsilon_1 = \frac{1}{N} \sum_{i=1}^{N} [y_i - \widehat{\mathscr{M}}_P(\boldsymbol{x}^i)]^2 \tag{17}$$

The well-known coefficient of determination R^2 reads

$$R^2 = 1 - \frac{\varepsilon_1}{V_y} \tag{18}$$

where V_y is the empirical variance of model responses $\boldsymbol{y}$. Even though the coefficient of determination can be easily obtained, it generally underestimates the true generalization error. An alternative approach for a more reliable estimate of generalization error is the leave-one-out (LOO) cross-validation, where the mean-square residual error is estimated by

$$\varepsilon_{LOO} = \frac{1}{N} \sum_{i=1}^{N} \left[y_i - \widehat{\mathscr{M}}_P^{\mathbf{X}\backslash i}(\boldsymbol{x}^{(i)}) \right]^2 \tag{19}$$

where $\widehat{\mathscr{M}}_P^{\mathbf{X}\backslash i}$ denotes a PCE model which is built from the DoE set $\mathbf{X}\backslash i = \{\boldsymbol{x}^1, \ldots, \boldsymbol{x}^{i-1}, \boldsymbol{x}^{i+1}, \ldots, \boldsymbol{x}^N\}^{\mathrm{T}}$ excluding $\boldsymbol{x}^i$. Thus the coefficient of determination Q^2 of leave-one-out cross-validation is estimated by

$$Q^2 = 1 - \frac{\varepsilon_{LOO}}{V_y} \tag{20}$$

Q^2 reflects the predictive ability of a metamodel. The method of

leave-one-out cross-validation performs well in the accuracy estimation of PCEs and is used to select the optimal PCE metamodel in this work.

According to Eq. (13), the number of PCE terms P grows exponentially with the problem dimension D and the PCE order p. Taking this study problem with 8 random variables as an example, a 5th-order full PCE has totally 1287 terms, which requires a DoE with more than 2500 samples. To enhance the computational efficiency of PCE, the method of relevance vector machine, in the framework of Bayesian inference, is adopted to estimate PCE coefficients. It does not only avoid the over-fitting problem caused by the least-square minimization method, but also give a sparse result of PCE.

6. Relevance vector machine

Relevance vector machine (RVM) is a Bayesian learning method for regression and classification tasks. Given a set of input vectors $\{\boldsymbol{x}^1, \boldsymbol{x}^2,\ldots, \boldsymbol{x}^N\}^{\mathrm{T}}$ and the corresponding output vector $\{y_1, y_2, \ldots, y_N\}^{\mathrm{T}}$, the aim of RVM is to find a parsimonious function $f(\boldsymbol{x}, \boldsymbol{w})$ to well represent the input-output relation with a good generalization performance,

$$y = f(\boldsymbol{x}, \boldsymbol{w}) + \varepsilon \tag{21}$$

where $\boldsymbol{w}$ is the weight vector, ε is a zero-mean normal random variable with the variance of ϑ^{-1}. Therefore, the model response y follows a Gaussian distribution,

$$p(y|\boldsymbol{w}, \boldsymbol{x}, \vartheta) = \mathcal{N}\left(f(\boldsymbol{x}, \boldsymbol{w}), \vartheta^{-1}\right) \tag{22}$$

Considering N input vectors $\{\boldsymbol{x}^1, \boldsymbol{x}^2, \ldots, \boldsymbol{x}^N\}^{\mathrm{T}}$ associated with N output $\{y_1, y_2, \ldots, y_N\}^{\mathrm{T}}$, a likelihood function is derived as,

$$p(\boldsymbol{y}|\boldsymbol{w}, \boldsymbol{x}, \vartheta) = \left(\frac{\vartheta}{2\pi}\right)^{N/2} \exp\left\{ -\frac{\vartheta}{2} \sum_{i=1}^{N} [y_i - f(\boldsymbol{x}_i, \boldsymbol{w})]^2 \right\} \tag{23}$$

In relevance vector machine, independent zero-mean Gaussian priori distributions are introduced to weight parameters w_i's with the variance of ζ_i^{-1}, and the likelihood of $\boldsymbol{w}$ is expressed as,

$$p(\boldsymbol{w}|\boldsymbol{\zeta}) = \left(\frac{1}{2\pi}\right)^{\frac{M}{2}} \prod_{i=1}^{M} \exp\left(-\frac{\zeta_i w_i^2}{2} \right) \tag{24}$$

where M represents the number of weight parameter, which is equal to the number of PCE coefficients in this work, and $\boldsymbol{\zeta} = \{\zeta_1, \zeta_2, \ldots, \zeta_M\}^{\mathrm{T}}$ is a vector of M hyperparameters which are the inverse variance of the associated weight w_i. According to the Bayes theorem, the posterior distribution of $\boldsymbol{w}$ is expressed as,

$$p(\boldsymbol{w}|\boldsymbol{y}, \boldsymbol{\zeta}, \vartheta) = \frac{p(\boldsymbol{y}|\boldsymbol{w}, \boldsymbol{x}, \vartheta) p(\boldsymbol{w}|\boldsymbol{\zeta})}{p(\boldsymbol{y}|\boldsymbol{\zeta}, \vartheta)} \tag{25}$$

where $p(\boldsymbol{y}|\boldsymbol{\zeta}, \vartheta)$ is a normalization term. As the likelihood and priori are both Gaussian distributions, the posterior distribution is also a Gaussian distribution,

$$p(\boldsymbol{w}|\boldsymbol{y}, \boldsymbol{\zeta}, \vartheta) = \mathcal{N}(\boldsymbol{\mu}_w, \boldsymbol{\Sigma}_w) \tag{26}$$

where

$$\mu_w = \vartheta \boldsymbol{\Sigma}_w \boldsymbol{\Psi}^T y \tag{27}$$

$$\boldsymbol{\Sigma}_w = (\mathbf{A} + \vartheta \boldsymbol{\Psi}^T \boldsymbol{\Psi})^{-1} \tag{28}$$

where $\mathbf{A} = \mathrm{diag}(\zeta_1, \zeta_2, \ldots \zeta_M)$. The values of hyperparametrs $\boldsymbol{\zeta}$ and ϑ can be obtained by maximization of the log marginal likelihood as follows,

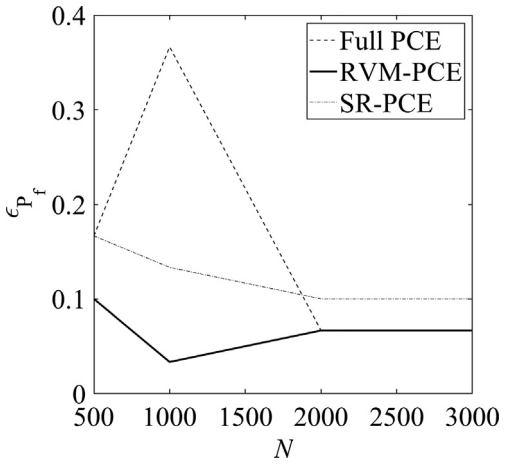

Fig. 3. Comparisons of estimated failure probabilities.

$$\mathscr{L}(\boldsymbol{\zeta}, \vartheta) = \ln \int p(\boldsymbol{y}|\boldsymbol{w}, \boldsymbol{x}, \vartheta) p(\boldsymbol{w}|\boldsymbol{\zeta}) d\boldsymbol{w} = -\frac{1}{2}\left(M \ln 2\pi + \ln|\boldsymbol{\Omega}| + \boldsymbol{y}^T \boldsymbol{\Omega}^{-1} \mathbf{y}\right) \tag{29}$$

where $\boldsymbol{\Omega} = \vartheta^{-1}\mathbf{I} + \boldsymbol{\Psi}\mathbf{A}^{-1}\boldsymbol{\Psi}^T$. An iteration algorithm was proposed by Tipping (2001) to find the optimal $\boldsymbol{\zeta}$ and ϑ. If the optimal ζ_i (the inverse variance of the coefficient w_i) becomes very large, the priori distribution of w_i is confined to a narrow range concentrating around zero, meaning that the weight parameter w_i has a high probability of being zero. With certain PCE coefficients being zero, this finally leads to a sparse representation of $f(\boldsymbol{x}, \boldsymbol{w})$.

7. RVM-PCE

This study combines the relevance vector machine with polynomial chaos expansion (RVM-PCE) to perform probabilistic analysis on seismic slope stability. The PCE terms, $\psi_i(\boldsymbol{x})$'s, are adopted as the basis functions in RVM, and a necessary condition of RVM is to predetermine the number of these functions (i.e. the order of PCE). In order to select the best PCE order, a maximum order $p_{\max}$ is first assigned, and a series of PCEs are built for each order $p = 1, \ldots, p_{\max}$ through RVM. The optimal PCE metamodel is selected as the one associated with the smallest ε_{LOO} (or the largest coefficients of determination Q^2 for the leave-one-out cross-validation).

It is worth noting that the proposed RVM-PCE approach differs from the stepwise regression (SR) algorithm (Blatman and Sudret, 2010) in various ways. In SR-PCE, in order to achieve a sparse PCE, the stepwise

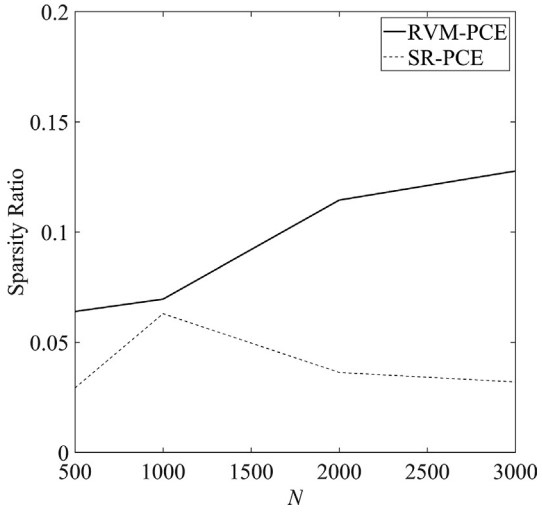

Fig. 4. Comparisons of sparsity ratio.

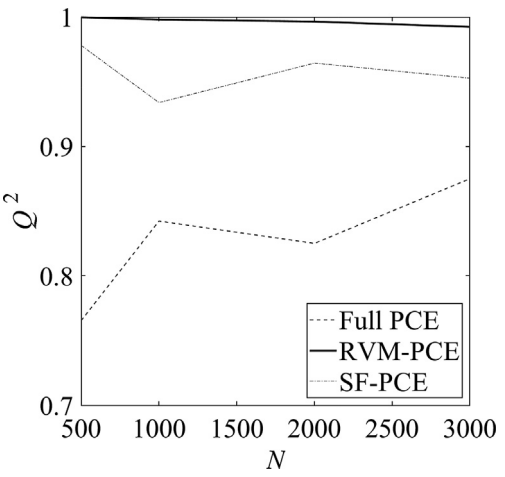

Fig. 5. Comparisons of coefficient of determination Q^2 of the leave-one-out cross-validation.

regression method is employed to identify important terms from a full PCE (discarding negligible terms), where an important term is one that leads to a significant change in the estimated coefficient of determinations. Meanwhile, the method of least square is used to estimate the coefficients of the retained PCE basis. In the proposed RVM-PCE, independent zero-mean Gaussian priori distributions are assigned to the weight parameters of the full PCE terms. Sparsity is achieved when the obtained variance of the Gaussian priori distribution of a weight parameter is very small, which means the corresponding weight parameter is equal to zero. The weight parameters (PCE coefficients) are determined by Bayesian regression method.

8. Comparisons with other metamodeling approaches

The applicability of the proposed method to the probabilistic analysis of seismic slope displacement is examined in this section. The proposed method is compared with full PCEs, and SR-PCE. The ground motion parameters of this case are taken from Tables 1 and 2, and the input parameters of slope A given in Table 3 are adopted. In the proposed RVM-PCE, the maximum PCE order p_{max} is set to 7. The failure probability estimated by MCS with 1.0×10^5 samples is equal to 6.3×10^{-3}, which is taken as the reference value. The relative errors with respect to the MCS reference value (ζ_{P_f}) for three different approaches are plotted in Fig. 3 when the number of DoE sample N changes from 500 to 3000. When the number of DoE samples is relatively small, e.g., less than 2000, RVM-PCE leads to the smallest relative errors of less than 10%, corresponding to the best estimations of failure probabilities, while full PCE produces the largest relative errors. This shows the superiority of the proposed RVM-PCE approach, especially when the available DoE samples are sparse (common in reality). The relative errors associated with three methods decrease with the increasing number of DoE samples. This is expected as the performance of a PCE metamodel should improve with the number DoE samples. When N exceeds 2000, both the full PCE and the proposed RVM-PCE converges to the same relative errors, while the SR-PCE produces the highest relative errors.

The SPCE sparsity ratio, which is the ratio of the number of retained terms in a SPCE to that of its full PCE counterpart, is presented in Fig. 4. The RVM-PCE has greater sparsity ratios than the SR-PCE, which means that a SPCE obtained by RVM has more retained terms than the one by SR-PCE. This is likely because the SR algorithm abandons some necessary terms, and this may also be the reason why the SR-PCE produces less accurate estimates of failure probabilities. The Q^2 value at different numbers of DoE samples are shown in Fig. 5. In all cases, the proposed RVM-PCE leads to the highest values of Q^2, meaning that the proposed RVM-PCE results in the lowest generalization errors on DoE samples, which contribute to its high accuracy when estimating failure probabilities. The proposed RVM-PCE is therefore adopted for the probabilistic analyses in later sections.

Table 5
Results of sobol' index analyses.

Variables	COV(I_a) = 1.0	COV(I_a) = 3.5
I_a	0.5842	0.8233
$D_{5\text{-}95}$	0.1087	0.1250
t_{mid}	0.0108	0.0309
ω_{mid}	0.0010	0.0026
ω'	0.0004	0.0001
ζ_f	0.0009	0.0002
φ	0.0062	0.0025
c	0.1229	0.0170

9. Sensitivity analysis

Sobol' indices are then evaluated to quantify the respective contribution or influence of each random variable to the system responses. Table 5 shows the obtained results of sensitivity analysis for slope A when the cohesion and friction angle are uncorrelated. Two different values of COVs for I_a are considered, which are 1.0 and 3.5. In both cases, the Sobol' index of I_a is the highest among all ground motion and soil parameters, indicating that I_a contributes the most to the seismically-induced slope displacements. This is partly because the Arias intensity is the primary indicator representing earthquake shaking amplitudes and durations, and partly because it has the largest COV compared with other variables. In the case of COV(I_a) = 1.0, the second most important variable is the soil cohesion, which is followed by $D_{5\text{-}95}$ and t_{mid}. When COV(I_a) = 3.5, the strong shaking duration $D_{5\text{-}95}$ becomes the second most important parameter, followed by t_{mid} and c. This shows that the strong shaking duration of the earthquake and soil strength parameters are also influential to seismic slope displacements. On the contrary, the frequency changing rate ω' and damping ratio ζ_f are the least important parameters. The Newmark-type displacement is more sensitive to the intensity and duration of ground motions than the frequency contents.

Fig. 6 shows the variations in mean estimates of Newmark-type displacements with four ground motion parameters (I_a, $D_{5\text{-}95}$, t_{mid}, ω_{mid}) for slope A. The effects of frequency changing rate ω' and bandwidth parameter ζ_f are not shown due to their insignificant influences. As expected, the mean values of displacements increase with I_a and $D_{5\text{-}95}$ (Fig. 6a and b). The relationship between the displacements and t_{mid} normalized by $D_{5\text{-}95}$ is shown in Fig. 6c, showing an increasing trend of displacements before $t_{mid}/D_{5\text{-}95}$ reaches the values of approximately 0.5–0.6, beyond which the displacements reduce with $t_{mid}/D_{5\text{-}95}$. Fig. 6d shows that the mean displacements increase sharply with ω_{mid} before 8 Hz, after which the rate of change is relatively low. This shows that the seismic slope displacements are more sensitive to low frequency contents of the ground motion.

10. Fragility curves for slope stability

In probabilistic seismic hazard analysis (PSHA), a hazard curve is used to show the relationship between a ground motion intensity measure and its mean annual probability of exceedance at a site. In this study, the hazard curve of Arias intensity is selected because it is the most influential to displacement predictions. Two hazard curves of I_a from two sites in California are given in Fig. 7 (Howard et al., 2008), where the annual exceedance probability decreases with the Arias intensity.

The failure probabilities of slopes with an allowable displacement of 10 cm are then evaluated using the RVM-PCE method. The mean values of Arias intensity μ_{I_a} is set to change from 0 to 10 m/s, and three mean values of $D_{5\text{-}95}$ (10 s, 17.25 s, and 25 s) are considered. The obtained failure probabilities, also referred to as fragility curves, are provided in Fig. 8a for the case of slope A and in Fig. 8b for the case of slope B. The

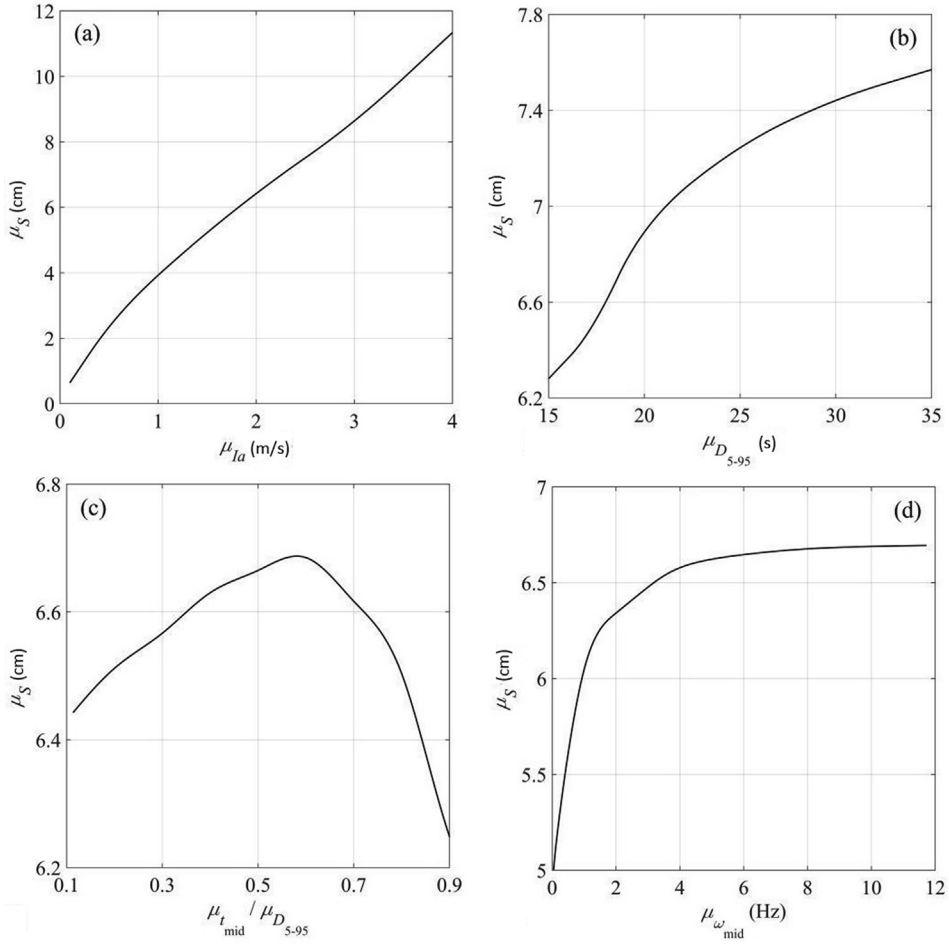

Fig. 6. Influences of four ground motion parameters, (a) I_a, (b) $D_{5\text{-}95}$, (c) t_{mid}, (d) ω_{mid}, on mean estimates of slope Newmark-type displacements.

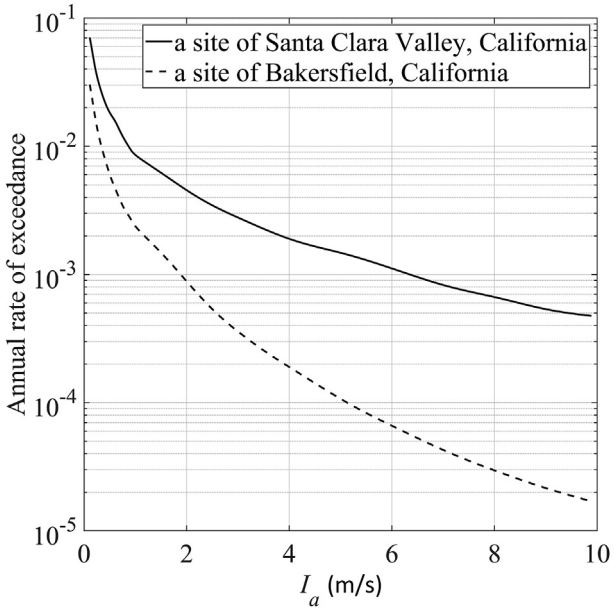

Fig. 7. PSHA hazard curves of Arias intensity.

obtained failure probability quickly increases with the Arias intensity before $\mu I_a = 4$ m/s, beyond which it increases more slowly. For example, in Fig. 8a, the failure probability increases more than a hundredfold from 2.5×10^{-3} at $\mu I_a = 0.1$ m/s to 3.5×10^{-1} at $\mu I_a = 4$ m/s (for $\mu_{D5\text{-}95} = 17.25$ s), and only increases by around 100% as μI_a rises from 4 m/s to 10 m/s.

The annual failure probability is equal to the product of the annual rate of occurrence of the Arias intensity and the associated fragility curves of slopes under that hazard level. Under the proposed framework, the hazard curves of the Arias intensity given in Fig. 7 and the fragility curves in Fig. 8 are employed to obtain the corresponding annual failure probabilities, which are plotted in Fig. 9. As shown in the figure, both I_a and $D_{5\text{-}95}$ have significant influences on the annual failure probabilities. It is interesting to note that the annual failure probability increases with the Arias intensity to a peak value and then decreases; this maximum annual failure probability occurs at a certain value of Arias intensity which corresponds to a relatively high annual rate of occurrence and a relatively large value of slope failure probability. In Fig. 9a, the most probable annual failure event occurs when μI_a is approximately equal to 2 m/s, while in Fig. 9b it happens at $\mu I_a = 0.6$ m/s. This shows that the highest risk in slope engineering design is not always associated with the largest Arias intensity. It is also important to consider the seismic hazard levels at the specific site.

11. Conclusions

This paper presents an approach that allows probabilistic analysis on

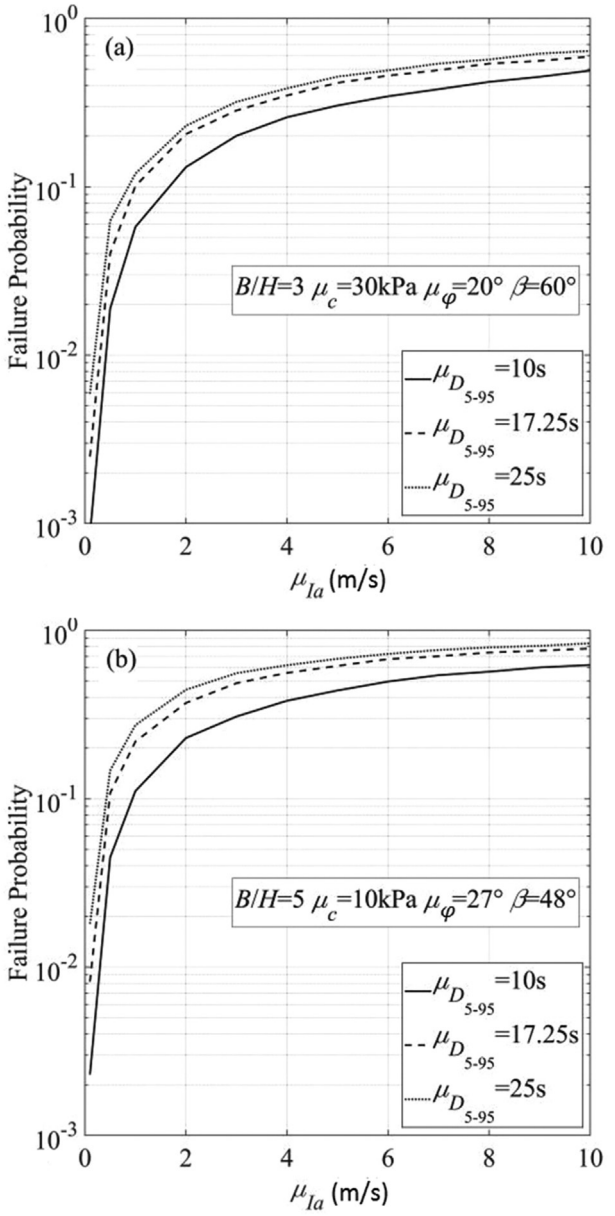

Fig. 8. Fragility curves as a function of Arias intensity for (a) $B/H = 3.0$, $\mu_c = 30$ kPa, $\mu_\varphi = 20°$, $\beta = 60°$ and (b) $B/H = 5.0$, $\mu_c = 10$ kPa, $\mu_\varphi = 27°$, $\beta = 48°$.

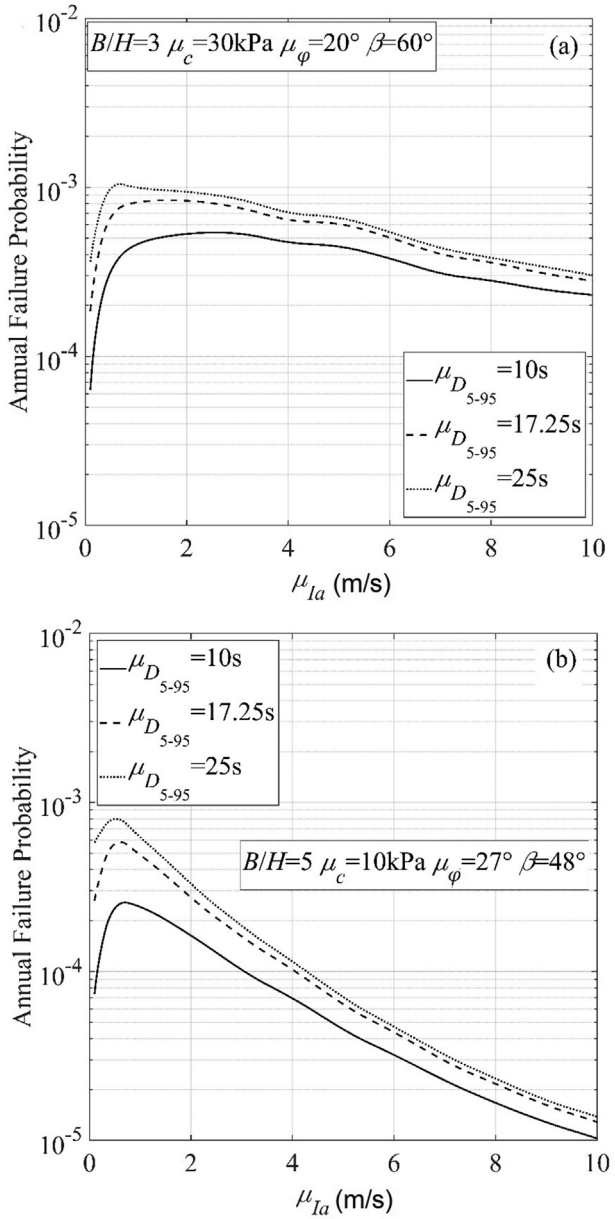

Fig. 9. Annual slope failure probabilities at (a) Santa Clara Valley site and (b) Bakersfield site.

seismic slope performance to be performed with rigorous considerations of uncertainties associated with earthquake ground motions and soil shear strength. The Rezaeian stochastic ground motion model enables the generation of acceleration time histories with realistic temporal and spectral non-stationary characteristics, and the corresponding ground motion parameters, including intensity, frequency and duration, have clear physical meanings related to the earthquake shaking features. By utilizing the 3D slope failure mechanism and Newmark-type displacement analysis method, the approach is more efficient than probabilistic analyses through finite element methods. In order to perform probabilistic analysis, a new metamodel that utilizes relevance vector machine and polynomial chaos expansion is proposed, showing better performance compared with previous PCE methods.

Quantitative sensitivity analyses indicate that the ground motion features of intensity and duration are more influential to the slope displacements, compared to the frequency contents. Interestingly, there is a critical magnitude of Arias intensity that is related to the maximum annual failure probability, as a result of the combined effects of PSHA hazard level and the slope failure probabilities. Such a critical Arias intensity should be carefully considered in earthquake slope engineering. The proposed method allows this critical magnitude to be determined rationally in site-specific assessments of slope safety under seismic conditions.

The failure mechanism (or the slip surface) is a critical assumption for slope stability assessments, which may eventually affect the results of failure probability evaluations. In this study, the 3D rotational failure mechanism is adopted to assess the critical seismic acceleration and Newmark-type displacements. The geometrical shape of the failure mechanism (or the slip surface) is determined by optimizing the upper-bound solution, equating the external work rates to the internal energy dissipations, in search of the critical seismic accelerations. Uncertainties in the size and shape of the slip surface are therefore not considered. This is a limitation of the current study and a potential area for future developments.

Declaration of competing interest

The authors declare that they have no known competing financial interests or personal relationships that could have appeared to influence the work reported in this paper.

Acknowledgements

The work presented in this paper is financially supported by the Research Grants Council of the Hong Kong Special Administrative Region (Project No. 15212418).

References

Al-Bittar, T., Soubra, A.H., Thajeel, J., 2018. Kriging-based reliability analysis of strip footings resting on spatially varying soils. J. Geotech. Geoenviron. Eng. 144 (10), 04018071.

Blatman, G., Sudret, B., 2010. An adaptive algorithm to build up sparse polynomial chaos expansions for stochastic finite element analysis. Probabilist. Eng. Mech. 25 (2), 183–197.

Blake, T.F., Hollingsworth, R.A., Stewart, J.P., 2002. Recommended procedures for implementation of DMG special publication 117 guidelines for analyzing and mitigating landslide hazards in California. Los Angeles Section Geotechnical Group, Southern California Earthquake Center.

California Geological Survey, 2008. Guidelines for Evaluating and Mitigating Seismic Hazards in California, 117A. California Geological Survey Special Publication, p. 98.

Campbell, K.W., Bozorgnia, Y., 2007. Campbell-bozorgnia NGA Ground Motion Relations for the Geometric Mean Horizontal Component of Peak and Spectral Ground Motion Parameters. PEER Report No. 2007/02, Pacific Earthquake Engineering Research Center. University of California, Berkeley, p. 238.

Campbell, K.W., Bozorgnia, Y., 2008. NGA ground motion model for the geometric mean horizontal component of PGA, PGV, PGD and 5% damped linear elastic response spectra for periods ranging from 0.01 to 10 s. Earthq. Spectra 24 (1), 139–171.

Chousianitis, K., Del Gaudio, V., Kalogeras, I., Ganas, A., 2014. Predictive model of Arias intensity and Newmark displacement for regional scale evaluation of earthquake-induced landslide hazard in Greece. Soil Dynam. Earthq. Eng. 65, 11–29.

Du, W., Wang, G., 2016. A one-step Newmark displacement model for probabilistic seismic slope displacement hazard analysis. Eng. Geol. 205, 12–23.

Ghanem, R., Spanos, P., 2003. Stochastic Finite Elements: A Spectral Approach, second ed. Dover, Mineola, NY.

Guo, X., Dias, D., Carvajal, C., Peyras, L., Breul, P., 2018. Reliability analysis of embankment dam sliding stability using the sparse polynomial chaos expansion. Eng. Struct. 174, 295–307.

He, Y., Hazarika, H., Yasufuku, N., Han, Z., Li, Y., 2015. Three-dimensional limit analysis of seismic displacement of slope reinforced with piles. Soil Dynam. Earthq. Eng. 77, 446–452.

Hsieh, S.Y., Lee, C.T., 2011. Empirical estimation of the Newmark displacement from the Arias intensity and critical acceleration. Eng. Geol. 122 (1–2), 34–42.

Howard, J.K., Fraser, W.A., Schultz, M.G., 2008. Probabilistic use of Arias Intensity in geotechnical earthquake engineering. In: Geotechnical Earthquake Engineering and Soil Dynamics Congress IV. Sacramento, California, United States, pp. 1–10.

Huang, F., Ou, R.C., Li, Z.L., Yang, X.L., Ling, T.H., 2018. Limit analysis for the face stability of a shallow-shield tunnel based on a variational approach to the blow-out failure mode. Int. J. GeoMech. 18 (6), 04018038. https://doi.org/10.1061/(ASCE)GM.1943-5622.0001150.

Jibson, R.W., Keefer, D.K., 1993. Analysis of the seismic origin of landslides: examples from the New Madrid seismic zone. Geol. Soc. Am. Bull. 105 (4), 521–536.

Jibson, R.W., Harp, E.L., Michael, J.A., 2000. A method for producing digital probabilistic seismic landslide hazard maps. Eng. Geol. 58 (3–4), 271–289.

Jibson, R.W., Michael, J.A., 2009. Maps showing seismic landslide hazards in Anchorage, Alaska. U.S. Geological Survey Scientific Investigations Map 3077.

Jibson, R.W., 2011. Methods for assessing the stability of slopes during earthquakes—a retrospective. Eng. Geol. 122 (1–2), 43–50.

Keefer, D.K., Wilson, R.C., 1989. Predicting earthquake-induced landslides, with emphasis on arid and semi-arid environments. In: Sadler, P.M., Morton, D.M. (Eds.), Landslides in a Semi-Arid Environment. Inland Geological Society. Riverside, CA, 2, 118–149.

Kim, J.M., Sitar, N., 2013. Probabilistic evaluation of seismically induced permanent deformation of slopes. Soil Dynam. Earthq. Eng. 44, 67–77.

Lin, J.S., Whitman, R.V., 1986. Earthquake induced displacements of sliding blocks. Journal of Geotechnical Engineering 112 (1), 44–59.

Li, Z., Jiang, Y., Tao, Z., He, M., 2018. Monitoring prediction of a rockslide in an open-pit mine and numerical analysis using a material instability criterion. Bull. Eng. Geol. Environ. 78, 2041–2053. https://doi.org/10.1007/s10064-017-1224-z.

Li, D., Chen, Y., Lu, W., Zhou, C., 2011. Stochastic response surface method for reliability analysis of rock slopes involving correlated non-normal variables. Comput. Geotech. 38 (1), 58–68.

Leshchinsky, B.A., 2018. Nested Newmark model to calculate the post-earthquake profile of slopes. Eng. Geol. 233, 139–145.

Lo, M.K., Leung, Y.F., 2017. Probabilistic analyses of slopes and footings with spatially variable soils considering cross-correlation and conditioned random field. J. Geotech. Geoenviron. Eng. 143 (9), 04017044.

Lo, M.K., Leung, Y.F., 2018. Reliability assessment of slopes considering sampling influence and spatial variability by Sobol' sensitivity index. J. Geotech. Geoenviron. Eng. 144 (4), 04018010.

Michalowski, R.L., Drescher, A., 2009. Three-dimensional stability of slopes and excavations. Geotechnique 59 (10), 839–850.

Michalowski, R.L., Martel, T., 2011. Stability charts for 3D failures of steep slopes subjected to seismic excitation. J. Geotech. Geoenviron. Eng. 137 (2), 183–189.

Mollon, G., Dias, D., Soubra, A.H., 2010. Probabilistic analysis of pressurized tunnels against face stability using collocation-based stochastic response surface method. J. Geotech. Geoenviron. Eng. 137 (4), 385–397.

Nadukuru, S.S., Michalowski, R.L., 2013. Three-dimensional displacement analysis of slopes subjected to seismic loads. Can. Geotech. J. 50 (6), 650–661.

Newmark, N.M., 1965. Effects of earthquakes on dams and embankments. Geotechnique 15 (2), 139–160.

Pan, Q., Dias, D., 2017. An efficient reliability method combining adaptive Support Vector Machine and Monte Carlo Simulation. Struct. Saf. 67, 85–95.

Pan, Q., Qu, X., Liu, L., Dias, D., 2020. A sequential sparse polynomial chaos expansion using Bayesian regression for geotechnical reliability estimations. Int. J. Nume. Anal. Meth. Geomech. 1 (32), 1–16. https://doi.org/10.1002/nag.3044.

Pan, Q., Xu, J, Dias, D., 2017. Three-dimensional stability of a slope subjected to seepage forces. Int. J. GeoMech., 04017035

Qin, C.B., Chian, S.C., 2018. Kinematic analysis of seismic slope stability with a discretisation technique and pseudo-dynamic approach: a new perspective. Geotechnique 68 (6), 492–503. https://doi.org/10.1680/jgeot.16.P.200.

Rezaeian, S., Der Kiureghian, A., 2008. A stochastic ground motion model with separable temporal and spectral nonstationarities. Earthq. Eng. Struct. Dynam. 37 (13), 1565–1584.

Rezaeian, S., 2010. Stochastic Modeling and Simulation of Ground Motions for Performance-Based Earthquake Engineering. University of California, Berkeley.

Sudret, B., 2008. Global sensitivity analysis using polynomial chaos expansions. Reliab. Eng. Syst. Saf. 93 (7), 964–979.

Tipping, M.E., 2001. Sparse Bayesian learning and the relevance vector machine. J. Mach. Learn. Res. 1, 211–244.

Travasarou, T., Bray, J.D., Der Kiureghian, A., 2004. A probabilistic methodology for assessing seismic slope displacements. In: 13th World Conf. On Earthquake Engineering. Vancouver, B.C., Canada. Paper No. 2326.

Tsai, C.C., Chien, Y.C., 2016. A general model for predicting the earthquake-induced displacements of shallow and deep slope failures. Eng. Geol. 206, 50–59.

Wan, H.P., Ren, W.X., Todd, M.D., 2017. An efficient metamodeling approach for uncertainty quantification of complex systems with arbitrary parameter probability distributions. Int. J. Numer. Methods Eng. 109 (5), 739–760.

Wieczorek, G.F., Wilson, R.C., Harp, E.L., 1985. Map showing slope stability during earthquakes in San Mateo County, California. U.S. Geological Survey Miscellaneous Investigations Map I-1257.

Xu, J., Kong, F., 2018. A cubature collocation based sparse polynomial chaos expansion for efficient structural reliability analysis. Struct. Saf. 74, 24–31.

Yang, X.L., Pan, Q.J., 2015. Three dimensional seismic and static stability of rock slopes. Geomechanics and Engineering 8 (1), 97–111.

Zhang, W.G., Goh, A.T.C., 2013. Multivariate adaptive regression splines for analysis of geotechnical engineering systems. Comput. Geotech. 48, 82–95.

Zhao, L.H., Zuo, S., Lin, Y.L., Li, L., Zhang, Y., 2016. Reliability back analysis of shear strength parameters of landslide with three-dimensional upper bound limit analysis theory. Landslides 13, 711–724.